
On Kernel-based Variational Autoencoder

Tian Qin

Math department
Lehigh University
Bethlehem, PA 18015
tjq218@lehigh.edu

Wei-Min Huang

Math department
Lehigh University
Bethlehem, PA 18015
wh02@lehigh.edu

Abstract

In this paper, we bridge Variational Autoencoders (VAEs) [14] and kernel density estimations (KDEs) [21, 19] by approximating the posterior by the expectation of kernel density estimator and deriving a new lower bound of empirical log likelihood. The flexibility of KDEs provides a new perspective of controlling the KL-divergence term in original evidence lower bound (ELBO) which enhances the flexibility of the posterior and prior pairs in VAE. We show that the Epanechnikov kernel gives the tightest upper bound in controlling the KL-divergence under appropriate conditions [7, 2] in theory and develop a kernel-based VAE called Epanechnikov Variational Autoencoder (EVAE). The implementation of Epanechnikov kernel in VAE is straightforward as it lies in the “location-scale” family of distributions where reparametrization tricks can be applied directly. Compared with Gaussian kernel, Epanechnikov kernel has compact support which should make the generated sample less blurry. Extensive experiments on benchmark datasets such as MNIST, Fashion-MNIST, CIFAR-10 and CelebA illustrate the superiority of Epanechnikov Variational Autoencoder (EVAE) over vanilla VAE and other baseline models in the quality of reconstructed images, as measured by the FID score and Sharpness [24].

1 Introduction

In variational inference, an autoencoder learns to encode the original data \mathbf{x} using learnable function $f_\phi^{-1}(\mathbf{x})$ and then to reconstruct x using a decoder g_θ . [14] proposed a stochastic variational inference and learning algorithm called Variational Autoencoders (VAEs) which can be further used to generate new data. According to VAE, a lower bound on the empirical likelihood, which is known as ELBO, is maximized so that the fitted model $p_\theta(\mathbf{x}|\mathbf{z}) = \mathcal{N}(\mathbf{x}; g_\theta(\mathbf{z}), I_D)$ and $q_\phi(\mathbf{z}|\mathbf{x}) = \mathcal{N}(\mathbf{z}; f_\phi(\mathbf{x}), I_D)$ can approximate the true conditional distributions $p(\mathbf{x}|\mathbf{z})$ and $p(\mathbf{z}|\mathbf{x})$, respectively. The isotropic Gaussian prior and posterior distribution in vanilla VAE is mathematically convenient since the corresponding ELBO is analytic. But the main drawbacks are the lack of expressibility of latent space and the possible posterior collapse. There are two popular directions for extending VAEs to address these drawbacks.

1.1 Approximate posterior $q_\phi(\mathbf{z}|\mathbf{x})$:

To enhance the posterior expressiveness, Normalizing flow (NF) [20] applies a sequence of invertible transformations to initial density $q_0(\mathbf{z})$ to achieve more expressive posteriors. β -VAE [12] introduced a new parameter β in balancing the reconstruction loss with disentangled latent representation $q_\phi(\mathbf{z}|\mathbf{x})$. Importance weighted Autoencoders (IWAE) [3] improved log-likelihood lower bound by importance weighting. It also approximated the posterior with multiple samples and enriched latent space representations. [22] proposed the Aggregate Variational Autoencoder (AVAE), which

estimates the posterior by Gaussian kernel density estimations (KDEs) to improve the quality of the learned latent space.

1.2 Prior distribution $p(\mathbf{z})$ of latent variable \mathbf{z} :

Instead of approximating posterior, we can replace Gaussian prior with other flexible distributions. For instance, [6] used a simple Gaussian mixture prior and [25] introduced a mixture prior called “VampPrior” which consists of a mixture distribution with components given by variational posteriors. The possibility of non-parametric priors is explored in [18], which utilized a truncated stick-breaking process. [10] and [4] attempted to replace Gaussian prior by von Mises-Fisher(vMF) distribution to cover hyperspherical latent space. For data with heavy-tailed characteristics, [13] replaced Gaussian prior with heavy-tailed distributions such as the Student’s t-distribution, which allows the model to capture data with higher kurtosis, leading to more robust representations. [9] utilized optimal transport theory design priors that enforce a coupling between the prior and data distribution.

Most variants of VAE along these two directions require the closed-form KL divergence. This is essential in implementation but somehow limits the potential applications of more flexible pairs of posterior and prior, which may have no closed-form of KL divergence but could better capture the latent data distribution and alleviate model collapse. To improve the flexibility of the choice of posterior and prior in VAE, in this paper, we estimate the posterior by the expectation of kernel density estimator and derive a corresponding upper bound of KL-divergence, which has closed-form for many distributions. Such elasticity makes the derivation of the optimal functional form of kernel possible and the implementation time efficient.

It is true we can simply employ Monte-Carlo simulation (MC) to approximate KL-divergence for complicated posteriors. But the price is the time efficiency. For example, [4] employed von Mises-Fisher (vMF) distribution instead of Gaussian to better capture latent hyperspherical structure. With uniform prior, their proposed Hyperspherical Variational Auto-Encoders(HVAE) has closed form of KL-divergence while sampling from von Mises-Fisher (vMF) distribution requires acceptance-rejection method, which can be time consuming for high-dimensional latent space. Additionally, [22] directly employed a Gaussian kernel density estimator to estimate the posterior, which requires a large number of samples and is time consuming to achieve decent performance. Our main contributions can be summarized as follows.

1. We formulate the latent space learning process in VAE as a problem of kernel density estimation. Inspired by the results in [2] , we then model the posterior by the expectation of corresponding kernel density estimator and derive an upper bound of KL-divergence, which has closed-form for many distributions. Some asymptotic results are established as well. See details in section 2.2 and 3
2. After that, we utilize the conclusion from [2] and show that the derived upper bound of KL-divergence is tightest when we employ Epanechnikov kernel. The derivation connects a quadratic functional with KL-divergence, which to our best knowledge, is the first attempt to bridge the concept of asymptotic distribution of KDEs with VAE.
3. Thanks to the reparametrization trick, the implementation of Epanechnikov kernel in VAE is straightforward. We conduct detailed comparisons between Epanechnikov VAE (EVAE) and Gaussian VAE in many benchmark image datasets under standard encoder-decoder structure. The extensive experiments not only demonstrate the superiority of EVAE over VAE and other baselines in the quality of reconstructed images, as measured by the FID score and Sharpness[24] but also illustrate that EVAE has reasonable time efficiency compared to VAE.

The remaining sections of this paper are organized as following schema. In section 2, we provide some preliminaries involving VAE and kernel density estimations. In section 3, we show that Epanechnikov kernel gives the tightest upper bound in bounding the KL-divergence in the functional sense under appropriate conditions. Based on results in section 3, we propose the Epanechnikov VAE (EVAE) in section 4. The comparisons between EVAE, vanilla VAE and other baselines in benchmark datasets are illustrated in section 5. Section 6 discusses few characteristics and limitations of EVAE and suggests some future directions. The broader impact statement is enclosed in Appendix H. The pytorch codes for the implementation of EVAE and experiments are available in supplementary

materials. All experiments are performed on a laptop with 12th Gen Intel(R) Core(TM) i7-12700H (2.30 GHz), 16.0 GB RAM and NVIDIA 4070 GPU.

2 Preliminary

2.1 VAE formulation

Consider a dataset $\mathbf{X} = \{\mathbf{x}^{(i)}\}_{i=1}^n$ consists of n i.i.d samples from space \mathcal{X} whose dimension is d . In VAE, we assume that every observed data $\mathbf{x}^{(i)} = (x_1^{(i)}, x_2^{(i)}, \dots, x_d^{(i)}) \in \mathcal{X}$ is generated by a latent variable $\mathbf{z}^{(i)} \in \mathcal{Z}$ whose dimension is p . Then the data generation process can be summarized in 2 steps. It first produces a variable $\mathbf{z}^{(i)}$ from some prior distributions $p(\mathbf{z})$. Then given the value of $\mathbf{z}^{(i)}$, an observed value $\mathbf{x}^{(i)}$ is generated from certain conditional distribution $p_\theta(\mathbf{x}|\mathbf{z})$. We typically assume $d > p$ and likelihood $p_\theta(\mathbf{x}|\mathbf{z})$ are differentiable distributions w.r.t θ and \mathbf{z} . To maximize the empirical log likelihood $\log p_\theta(\mathbf{x})$, we need to evaluate the integral in the form

$$\log p_\theta(\mathbf{x}) = \log \int p_\theta(\mathbf{x}, \mathbf{z}) d\mathbf{z} = \log \int p_\theta(\mathbf{x}|\mathbf{z}) p(\mathbf{z}) d\mathbf{z},$$

which is intractable in most cases. Fortunately, we can instead maximizing its log evidence lower bound (ELBO) \mathcal{L} with the help of Jensen's inequality:

$$\log p_\theta(\mathbf{x}) \geq \mathbb{E}_{\mathbf{z} \sim q_\phi(\cdot|\mathbf{x})} [\log p_\theta(\mathbf{x}|\mathbf{z})] - KL(q_\phi(\mathbf{z}|\mathbf{x})||p(\mathbf{z})), \quad (1)$$

where the RHS of inequality (1) is called evidence lower bound (ELBO) and $KL(\cdot||\cdot)$ represents the KL-divergence between two distributions.

The conditional likelihood $p_\theta(\mathbf{x}|\mathbf{z})$, approximate posterior $q_\phi(\mathbf{z}|\mathbf{x})$ and the prior distribution $p(\mathbf{z})$ can be chosen independently. For convenience, most applications of VAE employ Gaussian parametrization for all three likelihoods. Since we would like to investigate new forms of posterior and prior rather than the form of conditional likelihood $p_\theta(\mathbf{x}|\mathbf{z})$, we can assume a multivariate Bernoulli or Gaussian model w.r.t $p_\theta(\mathbf{x}|\mathbf{z})$ for simplicity. For example, under multivariate Gaussian, we have $\log p_\theta(\mathbf{x}|\mathbf{z}) = \log \mathcal{N}(\mathbf{x}; g_\theta(\mathbf{z}), I)$. As to multivariate Bernoulli model, we have $\log p_\theta(\mathbf{x}|\mathbf{z}) = \sum_{i=1}^d [x_i \log(g_\theta(\mathbf{z})_i) + (1 - x_i) \log(1 - g_\theta(\mathbf{z})_i)]$ where $g_\theta(\mathbf{z}) : \mathcal{Z} \rightarrow \mathcal{X}$ are typically neural-network parametrizations.

To maximize ELBO, we now need to minimize the following target function for given data \mathbf{x} :

$$\mathbb{E}_{\mathbf{z} \sim q_\phi(\cdot|\mathbf{x})} [-\log p_\theta(\mathbf{x}|\mathbf{z})] + KL(q_\phi(\mathbf{z}|\mathbf{x})||p(\mathbf{z})). \quad (2)$$

The two terms in equation (2) are named as “reconstruction error” and “divergence” or “regularization term”, respectively. The “divergence” term regularizes the mismatch between approximate posterior and prior distribution.

2.2 Model the posterior as the expectation of kernel density estimator

A common assumption of latent space in VAE is the factorization of approximate posterior, i.e. dimensions of latent space are independent with each other. Under this assumption, we only need to consider the KDE formulation for posterior $q_\phi(\mathbf{z}|\mathbf{x})$ and prior $p(\mathbf{z})$ in one-dimensional case. Similar arguments can be applied to multi-dimensional cases by additivity of KL-divergence under independence. For the consistency of notations, we still use bold letter \mathbf{x} and \mathbf{z} to denote x and z in one-dimensional KDE. Given Y_1, \dots, Y_m be i.i.d random variables with a continuous density function f , [19, 21] proposed kernel density estimate $f_m(y)$ for estimating $f(y)$ at a fixed point $y \in \mathbb{R}$:

$$f_m(y) = \frac{1}{mb(m)} \sum_{i=1}^m K \left[\frac{y - Y_i}{b(m)} \right] = \frac{1}{b(m)} \int K \left[\frac{y - t}{b(m)} \right] dF_m(t), \quad (3)$$

where F_m is the sample distribution function, K is an appropriate kernel function such that $\int K(y) dy = 1$ and the positive number b_m , which typically relies on the sample size m , is called bandwidth such that $b(m) \rightarrow 0, mb(m) \rightarrow \infty$ as $m \rightarrow \infty$ ¹.

¹We omit the limits of integrals if they are $-\infty$ to ∞ .

On the other hand, with inequality $\log(t) \leq t - 1$ (for $t > 0$) we can bound KL-divergence as follows:

$$KL(q||p) = \int q(\mathbf{z}) \log \frac{q(\mathbf{z})}{p(\mathbf{z})} d\mathbf{z} \leq \int q(\mathbf{z}) \left(\frac{q(\mathbf{z})}{p(\mathbf{z})} - 1 \right) d\mathbf{z} = \int \frac{(q(\mathbf{z}) - p(\mathbf{z}))^2}{p(\mathbf{z})} d\mathbf{z}. \quad (4)$$

Let the posterior $q_\phi(\mathbf{z}|\mathbf{x}) = \mathbb{E}_0(q_{m,\phi}(\mathbf{z}))$, where

$$q_{m,\phi}(\mathbf{z}) = \frac{1}{mb(m)} \sum_{j=1}^m K_{\phi,\mathbf{x}} \left[\frac{\mathbf{z} - \mathbf{Z}_j}{b(m)} \right], \quad \mathbf{Z}_j \stackrel{i.i.d.}{\sim} p(\tilde{\mathbf{z}}).$$

is a kernel density estimator of $q_\phi(\mathbf{z}|\mathbf{x})$ with kernel $K_{\phi,\mathbf{x}}$, given KDE sample size m , data point \mathbf{x} and parameter ϕ . Expectation \mathbb{E}_0 is taken w.r.t the samples from prior distribution $p(\tilde{\mathbf{z}})$. In other words, we model the posterior as the expectation of the kernel density estimator. The subscript ϕ of kernel function implies that the parameters in kernel can be learned by neural networks.

By inequality (4) and Jensen inequality, we obtain

$$KL(q_\phi(\mathbf{z}|\mathbf{x})||p(\mathbf{z})) \leq \int \frac{[\mathbb{E}_0(q_{m,\phi}(\mathbf{z})) - p(\mathbf{z})]^2}{p(\mathbf{z})} d\mathbf{z} \leq \mathbb{E}_0 \left[\int \frac{(q_{m,\phi}(\mathbf{z}) - p(\mathbf{z}))^2}{p(\mathbf{z})} d\mathbf{z} \right]. \quad (5)$$

To this end, we obtain a new lower bound of log-likelihood of data:

$$\begin{aligned} \log p_\theta(\mathbf{x}) &\geq \mathbb{E}_{q_\phi(\mathbf{z}|\mathbf{x})} [\log p_\theta(\mathbf{x}|\mathbf{z})] - KL(q_\phi(\mathbf{z}|\mathbf{x})||p(\mathbf{z})) \\ &\geq \mathbb{E}_{q_\phi(\mathbf{z}|\mathbf{x})} [\log p_\theta(\mathbf{x}|\mathbf{z})] - \mathbb{E}_0 \left[\int \frac{(q_{m,\phi}(\mathbf{z}) - p(\mathbf{z}))^2}{p(\mathbf{z})} d\mathbf{z} \right]. \end{aligned} \quad (6)$$

Since we model the posterior as the expectation of the kernel density estimator, the number of latent variable Z generated from prior distribution, which is m , is just used for theoretical derivation and we found that sampling latent variable Z once is good enough in practice, as suggested by [14].

In the kernel density estimation theory, [7] showed that the Epanechnikov kernel minimizes $\int \mathbb{E}_0[q_{m,\phi}(\mathbf{z}) - p(\mathbf{z})]^2 d\mathbf{z}$ asymptotically, which gives us a hint of the functional optimization of kernel K in right hand side of inequality (5). The main assumptions of deriving optimal functional form of kernel are enclosed in Appendix A.

3 Choice of kernel

Let $f_m(t)$ be a kernel density estimate of a continuous density function f at t , as defined in equation (3), we construct a statistic T_m as follows:

$$T_m = mb(m) \int [f_m(t) - f(t)]^2 a(t) dt,$$

where $a(t)$ is an appropriate weight function. We now restate the main result of [2] as Theorem 3.1:

Theorem 3.1 (Bickel & Rosenblatt [2]) *Let assumptions **A1 – A4** in Appendix A hold and suppose that the weight function a is integrable piecewise continuous and bounded. Suppose $b(n) = o(n^{-\frac{2}{9}})$ and $o(b(n)) = n^{-\frac{1}{4}}(\log(n))^{\frac{1}{2}}(\log\log n)^{\frac{1}{4}}$ as $n \rightarrow \infty$, then $b^{-\frac{1}{2}}(n)(T_n - I(K) \int f(t)a(t)dt)$ is asymptotically normally distributed with mean 0 and variance $2J(K) \int a^2(t)f^2 dt$ as $n \rightarrow \infty$, where*

$$I(K) = \int K^2(t) dt, \quad J(K) = \int \left[\int K(t+y)K(t) dt \right]^2 dy. \quad (7)$$

In other words, under Theorem 3.1, we have

$$\mathbb{E}[T_m] \rightarrow I(K) \int f(t)a(t)dt \quad , \text{ as } m \rightarrow \infty .$$

Let $mb(m)/n = 1$ and $b(m)$ satisfies the conditions in Theorem 3.1, by the asymptotic result of Theorem 3.1, the inequality (5) becomes²:

$$\begin{aligned} KL(q_\phi(\mathbf{z}|\mathbf{x})||p(\mathbf{z})) &\leq \frac{mb(m)}{n} \mathbb{E}_0 \left[\int \frac{(q_{m,\phi}(\mathbf{z}) - p(\mathbf{z}))^2}{p(\mathbf{z})} d\mathbf{z} \right] \\ &= \frac{1}{n} \mathbb{E}_0 \left[mb(m) \int \frac{(q_{m,\phi}(\mathbf{z}) - p(\mathbf{z}))^2}{p(\mathbf{z})} d\mathbf{z} \right] \\ &\stackrel{n \text{ large}}{\approx} \frac{I(K_{\phi,\mathbf{x}}) \int p(\mathbf{z}) \frac{1}{p(\mathbf{z})} d\mathbf{z}}{n} = B \frac{I(K_{\phi,\mathbf{x}})}{n} , \end{aligned} \quad (8)$$

where B is the length of support interval of prior $p(\mathbf{z})$. For simplicity, we assume all data points have the same length of support interval. Note that if the prior has infinite length of support, the inequality (8) becomes theoretically useless. However, in practice, we found that parameter B is still useful for Gaussian prior. See Appendix G.2. We can now find the kernel which gives the tightest upper bound of KL-divergence i.e. the kernel $K_{\phi,\mathbf{x}}^*$ minimizing $I(K_{\phi,\mathbf{x}})$ given fixed parameters and data point \mathbf{x} . Lemma 3.2 shows that Epanechnikov kernel is the optimal choice.

Lemma 3.2 *Let \mathcal{K} be the set of all $L^1(-\infty, \infty)$ nonnegative functions K satisfying*

$$\int K(t)dt = 1, \int tK(t)dt = \mu, \int (t - \mu)^2 K(t)dt = \frac{1}{5}r^2$$

where $\mu \in (-\infty, \infty)$, $r > 0$. Then the functional $I(K)$ in equation (7) is minimized on \mathcal{K} uniquely by

$$K^*(t) = \begin{cases} \frac{3}{4r} \left(1 - \left(\frac{t-\mu}{r} \right)^2 \right) & t \in [\mu - r, \mu + r] \\ 0 & \text{otherwise} \end{cases}$$

and $\min_K I(K) = I(K^) = \frac{3}{5r}$. The optimal kernel K^* is named as Epanechnikov kernel [7].*

The proof is based on the idea of Lagrange multiplier. See Appendix B.1.

4 Epanechnikov VAE

Getting inspired by the functional optimality of Epanechnikov kernel in controlling KL-divergence, we propose the Epanechnikov Variational Autoencoder (EVAE) whose resampling step is based on Epanechnikov kernel. There are two main differences between EVAE and VAE. The latent distribution in EVAE is assumed to be estimated by the Epanechnikov kernel rather than multivariate isotropic Gaussian. And EVAE is trained to minimize a different target function (9):

$$\mathbb{E}_{z \sim q_{\phi(\cdot|\mathbf{x})}} [-\log p_\theta(\mathbf{x}|\mathbf{z})] + B \frac{I(K_{\phi,\mathbf{x}}^*)}{n} , \quad (9)$$

where n can be the sample size or minibatch size, ϕ are outputs of the encoding network, $K_{\phi,\mathbf{x}}^*$ is Epanechnikov kernel given data point \mathbf{x} and trainable neural network parameter ϕ , and support parameter B is a constant. Note that target function (9) is an upper bound of equation (2) used in ordinary VAE. Suppose we have M data points in each minibatch, the sample version of equation (9) at i -th data point $\mathbf{x}^{(i)}$ is

$$\tilde{\mathcal{L}}(\theta, \phi, \mathbf{B}; \mathbf{x}^{(i)}) \approx -\frac{1}{L} \sum_{l=1}^L (\log p_\theta(\mathbf{x}^{(i)}|\mathbf{z}^{(i,l)}) + \frac{3B}{5M} \sum_{k=1}^p \frac{1}{r_k^{(i)}}) , \quad (10)$$

²For the consistency of notations, we still use bold \mathbf{x} and \mathbf{z} to denote one-dimensional variable x and z in inequality ((8)) under the context of Theorem 3.1.

where $i \in \{1, 2, \dots, M\}$, p is the dimension for latent space, B is the support length of prior (which we set to be constant for each hidden dimension and all data points), $\mu^{(i)} = (\mu_1^{(i)}, \dots, \mu_p^{(i)})$, $\mathbf{r}^{(i)} = (r_1^{(i)}, \dots, r_p^{(i)})$ ³ are outputs of the encoding networks with variational parameters ϕ and M is minibatch size. In vanilla VAE, [14] suggested that the number of regenerated samples L can be set to 1 as long as the minibatch size is relatively large. Based on our experiment experience, this is also the case for EVAE. To sample latent variables from the posterior, we need to derive the density of $q_\phi(\mathbf{z}|\mathbf{x}^{(i)})$:

$$\begin{aligned} q_\phi(\mathbf{z}|\mathbf{x}^{(i)}) &= \mathbb{E}_0 \left[\frac{1}{mb(m)} \sum_{j=1}^m K_{\phi, \mathbf{x}^{(i)}}^* \left(\frac{\mathbf{z} - \mathbf{Z}_j}{b(m)} \right) \right] \\ &= \mathbb{E}_0 \left[\frac{1}{b(m)} K_{\phi, \mathbf{x}^{(i)}}^* \left(\frac{\mathbf{z} - \mathbf{Z}_1}{b(m)} \right) \right] \\ &= \int \frac{1}{b(m)} K_{\phi, \mathbf{x}^{(i)}}^* \left(\frac{\mathbf{z} - \tilde{\mathbf{z}}}{b(m)} \right) p_{\mathbf{z}}(\tilde{\mathbf{z}}) d\tilde{\mathbf{z}}, \end{aligned} \quad (11)$$

where $p_{\mathbf{z}}$ is the density of prior distribution. Given a data point $\mathbf{x}^{(i)}$, let $q_\phi(\mathbf{z}|\mathbf{x}^{(i)})$ be the density of random variable $Z(\mathbf{x}^{(i)})$, $K_{\phi, \mathbf{x}^{(i)}}^*$ be the density of random variable $K^*(\mathbf{x}^{(i)})$ and prior $p_{\mathbf{z}}$ is density of the random variable Z , then it's clear to see that the posterior is now a convolution between two random variables, i.e.

$$Z(\mathbf{x}^{(i)}) = b(m)K^*(\mathbf{x}^{(i)}) + Z. \quad (12)$$

Essentially, identity (12) decomposes the posterior into two parts. One is the prior information, the other represents the incremental updates from new information induced by data $\mathbf{x}^{(i)}$. The Epanechnikov kernel can be viewed as the “optimal” direction of perturbing the prior distribution and the coefficient $b(m)$ can be interpreted as “step size”, which controls the deviation of posterior from the prior. The resampling step in EVAE can be divided into two parts as well, as described in Algorithm 1 where we used uniform distribution as the prior in EVAE. For the sake of finite support and simplicity, we assume that the prior distribution is uniformly distributed and step size $b(m)$ is the same for all dimensions. The theoretical conditions for $b(m)$ is demanding. In practice we found that setting coefficient $b(m)$ as $b(100) = 100^{-2/9} \approx 0.3594$ is good enough.

Algorithm 1 Resampling step in a minibatch of EVAE

Require: Latent space dimension d_z ; Minibatch size M . Step size $b(m)$. Prior support interval length B . Mean $\mu_\phi(\mathbf{x})$, spread $\mathbf{r}_\phi(\mathbf{x})$ are all learned by encoder networks given input \mathbf{x} and have dimension $M \times d_z$.

- 1: Sample a $M \times d_z$ matrix \mathbf{U} where each (i, j) entry of the random matrix \mathbf{U} is sampled from $\text{Unif}[-B/2, B/2]$.
- 2: Sample a $M \times d_z$ matrix \mathbf{K} where each (i, j) entry of the random matrix \mathbf{K} is sampled from a standard Epanechnikov kernel supported on $[-1, 1]$.
- 3: Shift and scale sampled \mathbf{K} by the location-scale formula: $\mathbf{Z} = \mu_\phi(\mathbf{x}) + \mathbf{r}_\phi(\mathbf{x}) \odot \mathbf{K}$.
- 4: **Return:** $b(m) \odot \mathbf{Z} + \mathbf{U}$

Algorithm 2 Sampling from centered Epanechnikov kernel supported on $[-1, 1]$

- 1: Sample $U_1, U_2, U_3 \stackrel{i.i.d}{\sim} \text{Unif}[-1, 1]$.
- 2: Set $U = \text{Median}(U_1, U_2, U_3)$
- 3: **Return:** U

In Algorithm 1, we apply reparametrization trick to sample \mathbf{z} from general Epanechnikov kernel, i.e $\mathbf{z}^{(i,l)} = \mu^{(i)} + \mathbf{r}^{(i)} \odot \mathbf{k}^{(l)}$, where $\mathbf{k}^{(l)}$ is sampled from standard Epanechnikov kernel supported on $[-1, 1]$ as it lies in the “location-scale” family. We use \odot to signify the element-wise product. There are many ways to sample from standard Epanechnikov kernel, such as accept-rejection method. For efficiency, we provide a faster sampling procedure in Algorithm 2. The theoretical proof is given in Appendix B.2.

³The encode network output $\mu^{(i)}$ is used to sample from Epanechnikov based posterior and only optimized in the reconstruction term.

5 Experiments

In this section, we will compare the proposed EVAE model with (vanilla) VAE whose posterior and prior are modelled by isotropic multivariate Gaussian in real datasets. To assess the quality of reconstructed images, we employ the Frechet Inception Distance (FID) score [11] to measure the distribution of reconstructed images with the distribution of real images. The lower, the better. Inception_v3 [23] is employed as default model to generate features of input images, which is a standard implementation in generative models. Unlike the unbounded support of Gaussian distribution, the compact support for Epanechnikov kernel could help EVAE generate less blurry images. To check this claim empirically, we calculated sharpness [24] for reconstructed images by a 3×3 Laplace filter. See more details in Appendix D.

5.1 Benchmark datasets

Table 1: VAE and EVAE results on CIFAR10 and CelebA datasets

| Datasets | CIFAR-10 | | | | CelebA | | | |
|----------|----------|-------|-----------|-------|-----------|-------|-----------|-------|
| | d_z | VAE | | EVAE | | VAE | Sharpness | EVAE |
| | | FID | Sharpness | FID | Sharpness | | | |
| | 8 | 230.1 | 0.0353 | 226.6 | 0.0337 | 198.7 | 0.0147 | 198.7 |
| | 16 | 181.4 | 0.0350 | 164.2 | 0.0355 | 152.5 | 0.0148 | 149.7 |
| | 32 | 149.7 | 0.0348 | 123.5 | 0.0359 | 110.1 | 0.0156 | 97.5 |
| | 64 | 144.7 | 0.0355 | 79.7 | 0.0369 | 77.2 | 0.0163 | 65.3 |

We trained EVAE and VAE on four benchmark datasets: MNIST [5], Fashion-MNIST [26], CIFAR-10 [15] and CelebA [17]. The detailed information for training parameters are attached in Appendix D. In terms of FID score, we observe that EVAE has an edge in high dimensions ($d_z = 32, 64$), indicating the better quality of reconstructed images from EVAE. Additionally, when $d_z = 64$, EVAE generates higher sharpness of reconstructed images for all datasets, as illustrated in Table 1. See more results in Appendix G.1. This result empirically justifies the positive effect of having compact support in posteriors and priors. As to CIFAR-10, EVAE has larger sharpness in high dimensions ($d_z = 32, 64$) while it is relatively mediocre in low dimensions. Possible reasons include low-resolution(blurriness) of original images and deficient expressibility of simple CNN models in low dimensions. But the validation reconstruction loss curves in Appendix F indeed authenticate the superiority of EVAE over benchmark datasets, including CelebA.

5.2 Reconstruction samples

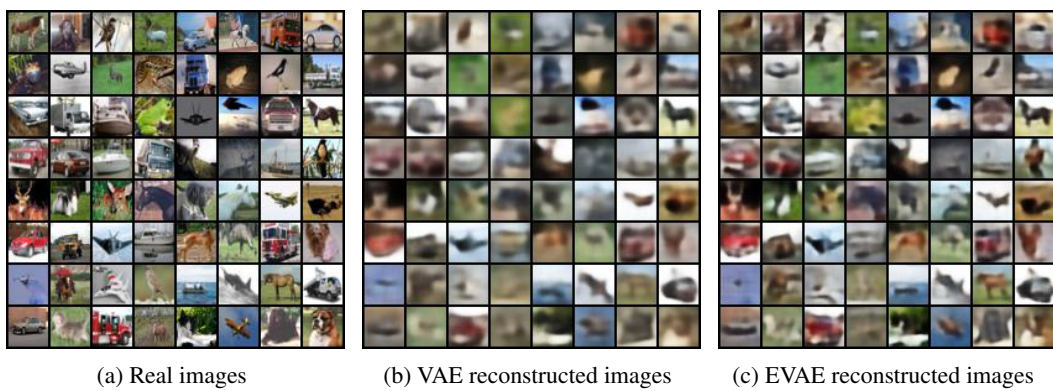


Figure 1: (a) Sampled real images from hold-out samples in CIFAR-10 (b) Reconstructed images by VAE. (c) Reconstructed images by EVAE. Dimension $d_z = 64$ for both models.

Figure 1 presents some test reconstructed samples from trained VAE and EVAE with $d_z = 64$ of CIFAR10, respectively. We can see many images reconstructed from EVAE are able to pick up local features better than the VAE. And reconstructed samples from CIFAR-10 are clearer and closer to the original images, as indicated by large gap between FID scores. See more examples of MINST, Fashion-MNIST and CelebA-64 datasets in Appendix E. The statistical analysis from binomial test based on total experiments (Appendix D) shows that EVAE significantly outperforms VAE in FID and sharpness.

5.3 Unconditional samples

Figure 2 demonstrates the unconditional samples from MINST dataset with EVAE⁴ and VAE and different values of parameter B. In other words, we directly sample from prior $p(z)$, multiply it by B and feed latent samples into decoder to obtain the unconditional samples. We observe that the larger the value of B is, the more diverse novel samples will be generated from EVAE. This makes sense as smaller value of B will make the model focus more on the perturbation part (KDE based) of identity (12), leading to the prior collapse. To this point, we can view the parameter B as a way to trade off the reconstruction and sample diversity.

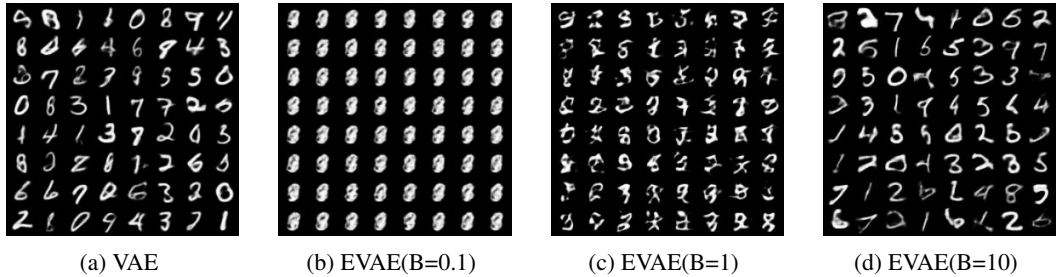


Figure 2: (a) Unconditional samples generated from VAE (MNIST dataset) (b) Unconditional samples generated from EVAE with B=0.1 (c) Unconditional samples generated from EVAE with B=1 (d) Unconditional samples generated from EVAE with B=10

5.4 Comparisons with baselines

In this section we conducted extra experiments comparing EVAE with open-source variants of VAE that improve the representational capacity of the encoder such as β -VAE [12], IWAE [3], WAE [24] and HVAE [4] on three datasets. Note that we didn't involve normalizing flow in the baselines as it belongs to a different type of image generation models. We employed uniform prior in EVAE and we ran all experiments for three times. We also reported mean and standard deviation of FID score (for testing set reconstruction quality). Same for sharpness. For fair comparisons, we used same encoder and decoder CNN architecture for all baselines. The only difference come from posterior modeling and prior modeling. All latent dimension d_z are set to be 64. Other hyperparameters and training details are the same with details in Appendix C and D.

From Table 2, we observe that EVAE with $B = 0.1$ performs universally good in FID and sharpness. Our support length parameter B plays the similar role with β in β -VAE, which verifies the intuition in the discussion section. In other words, B and β somehow control the reconstruction quality and sample diversity. For other baselines, WAE(MMD) performs also well in many cases, which is expected as it generalizes the KL divergence to the Wasserstein distance. IWAE has decent performance by utilizing importance weight sampling to shrink the gap between ELBO and log-likelihood, where $k = 5$ represents the number of samples in the importance sampling step. Hyperspherical VAE(HVAE) seems mediocre in our experiments, which might be due to the complexity of von-Mises Fisher prior and choice of dimension of hypersphere manifold. All the methods shared similar running time except for HVAE as it requires acceptance-rejection method for the sampling step, which is relatively time consuming for high-dimensional case.

⁴We employed uniform prior in the rest of experiments. Appendix G.2 already showed that there is no big difference for the model performance between uniform prior and Gaussian prior. The training details follows Appendix C and D.

Table 2: EVAE and other baselines

| Models | Fashion-MNIST | | CIFAR10 | |
|-------------------------------|------------------|----------------------|------------------|--------------------|
| | FID | Sharpness | FID | Sharpness |
| VAE | 39.1(0.3) | 0.016(3E-4) | 142.9(1.7) | 0.035(7E-4) |
| EVAE($B = 0.1$) | 12.2(0.2) | 0.027(2.1E-4) | 79.7(0.1) | 0.036(7E-4) |
| EVAE($B = 10$) | 32.6(0.5) | 0.019(4E-4) | 154.8(2.6) | 0.035(6E-4) |
| β -VAE($\beta = 0.1$) | 19.5(0.5) | 0.023(5E-4) | 84.4(0.8) | 0.035(5E-4) |
| β -VAE($\beta = 5$) | 74.5(2.0) | 0.01(2E-4) | 239.8(1.9) | 0.034(1.4E-3) |
| IWAE($k = 5$) | 26.8(0.1) | 0.02(3E-4) | 125.4(1.6) | 0.036(7E-4) |
| WAE(MMD) | 22.1(0.5) | 0.021(6E-4) | 140.1(7.2) | 0.034(7E-4) |
| HVAE | 36.8(0.3) | 0.016(1E-4) | 195.2(0.8) | 0.035(1E-3) |

5.5 Extra experiments

For completeness, we conducted extra experiments to see the performance of EVAE with Gaussian prior, effect of uniform prior support parameter B and the time efficiency of EVAE in Appendix G. In short, Appendix G.2 implies that the choice of prior doesn't effect the performance of EVAE very much. Appendix G.3 shows that the support parameter B plays an role in controlling the reconstruction quality. And Table 7 in Appendix G.4 verifies that EVAE is time efficient due to its simple implementation.

6 Discussion and limitation

6.1 Connections between EVAE and β -VAE

From target function (10), we can view the ratio $\frac{B}{M}$ can as a weight parameter in penalizing the kernel term. This formula is similar to the ELBO given in β -VAE. It would be interesting to compare the disentanglement and implicit regularization effect [16] of EVAE and β -VAE. In fact, in EVAE the weight parameter $\frac{B}{M}$ is derived from the global deviation result for KDEs, i.e. Theorem 3.1, where the constant B should be interpreted as the length of support interval for the prior.

On the other hand, the limitations of EVAE involve following few points:

6.2 A more precise approximation of KL-divergence

In section 2.2, we bounded the KL-term by a simple inequality $\log t \leq 1 - t$, which limits the potential of EVAE in more complicated cases such as high resolution images. It's possible to derive sharper bounds with higher order approximation where the Epanechnikov kernel may not be the optimal one.

6.3 Optimal kernel under different criterions

In this paper, we mainly focused on the L_2 deviation of KDEs, which is measured by the functional $I(K)$ proposed in Theorem 3.1. However, in the general theory of KDEs, different criterions lead to different optimal kernels. For example, we didn't put too much attention on the convolution functional $J(K) = \int [\int K(t+y)K(t)dt]^2 dy$, which is related to the asymptotic variance of statistic T_m defined in section 3. If we want to minimize the asymptotic variance of T_m , the optimal kernel is just the uniform kernel, as derived by [8].

In addition, the Bickel-Rosenblatt statistic T_m we defined in section 3 is proposed by [2], which can be viewed as a "continuous version" of the ordinary k-cell Chi-Square statistic and the KL-divergence is also a type of Chi-Square function [1]. Replacing KL-divergence with expectation of another type of Chi-Square statistic makes the kernel optimization (minimum Chi-Square estimation) in section 3 possible, which supports the claim in [1] that minimum Chi-Square estimate is more general and flexible.

References

- [1] Joseph Berkson. Minimum Chi-Square, not Maximum Likelihood! *The Annals of Statistics*, 8(3):457 – 487, 1980.
- [2] P. J. Bickel and M. Rosenblatt. On Some Global Measures of the Deviations of Density Function Estimates. *The Annals of Statistics*, 1(6):1071 – 1095, 1973.
- [3] Yuri Burda, Roger Baker Grosse, and Ruslan Salakhutdinov. Importance weighted autoencoders. *CoRR*, abs/1509.00519, 2015.
- [4] Tim R. Davidson, Luca Falorsi, Nicola De Cao, Thomas Kipf, and Jakub M. Tomczak. Hyper-spherical variational auto-encoders. *ArXiv*, abs/1804.00891, 2018.
- [5] Li Deng. The mnist database of handwritten digit images for machine learning research. *IEEE Signal Processing Magazine*, 29(6):141–142, 2012.
- [6] Nat Dilokthanakul, Pedro A. M. Mediano, Marta Garnelo, M. J. Lee, Hugh Salimbeni, Kai Arulkumaran, and Murray Shanahan. Deep unsupervised clustering with gaussian mixture variational autoencoders. *ArXiv*, abs/1611.02648, 2016.
- [7] V. A. Epanechnikov. Non-parametric estimation of a multivariate probability density. *Theory of Probability & Its Applications*, 14(1):153–158, 1969.
- [8] B. K. Ghosh and Wei-Min Huang. The Power and Optimal Kernel of the Bickel-Rosenblatt Test for Goodness of Fit. *The Annals of Statistics*, 19(2):999 – 1009, 1991.
- [9] Xiaoran Hao and Patrick Shafto. Coupled variational autoencoder. In Andreas Krause, Emma Brunskill, Kyunghyun Cho, Barbara Engelhardt, Sivan Sabato, and Jonathan Scarlett, editors, *Proceedings of the 40th International Conference on Machine Learning*, volume 202 of *Proceedings of Machine Learning Research*, pages 12546–12555. PMLR, 23–29 Jul 2023.
- [10] Abul Hasnat, Julien Bohné, Jonathan Milgram, Stéphane Gentric, and Liming Chen. von mises-fisher mixture model-based deep learning: Application to face verification. *ArXiv*, abs/1706.04264, 2017.
- [11] Martin Heusel, Hubert Ramsauer, Thomas Unterthiner, Bernhard Nessler, and Sepp Hochreiter. Gans trained by a two time-scale update rule converge to a local nash equilibrium. In *Proceedings of the 31st International Conference on Neural Information Processing Systems*, NIPS’17, page 6629–6640, Red Hook, NY, USA, 2017. Curran Associates Inc.
- [12] Irina Higgins, Loïc Matthey, Arka Pal, Christopher P. Burgess, Xavier Glorot, Matthew M. Botvinick, Shakir Mohamed, and Alexander Lerchner. beta-vae: Learning basic visual concepts with a constrained variational framework. In *International Conference on Learning Representations*, 2016.
- [13] Juno Kim, Jaehyuk Kwon, Mincheol Cho, Hyunjong Lee, and Joong-Ho Won. t^3 -variational autoencoder: Learning heavy-tailed data with student’s t and power divergence. In *The Twelfth International Conference on Learning Representations*, 2024.
- [14] Diederik P. Kingma and Max Welling. Auto-encoding variational bayes. *CoRR*, abs/1312.6114, 2013.
- [15] Alex Krizhevsky. Learning multiple layers of features from tiny images. Technical report, 2009.
- [16] Abhishek Kumar and Ben Poole. On implicit regularization in β -VAEs. In Hal Daumé III and Aarti Singh, editors, *Proceedings of the 37th International Conference on Machine Learning*, volume 119 of *Proceedings of Machine Learning Research*, pages 5480–5490. PMLR, 13–18 Jul 2020.
- [17] Ziwei Liu, Ping Luo, Xiaogang Wang, and Xiaou Tang. Deep learning face attributes in the wild. In *ICCV*, pages 3730–3738. IEEE Computer Society, 2015.
- [18] Eric Nalisnick and Padhraic Smyth. Stick-breaking variational autoencoders. In *International Conference on Learning Representations*, 2017.
- [19] Emanuel Parzen. On Estimation of a Probability Density Function and Mode. *The Annals of Mathematical Statistics*, 33(3):1065 – 1076, 1962.
- [20] Danilo Jimenez Rezende and Shakir Mohamed. Variational inference with normalizing flows. *ArXiv*, abs/1505.05770, 2015.

- [21] Murray Rosenblatt. Remarks on Some Nonparametric Estimates of a Density Function. *The Annals of Mathematical Statistics*, 27(3):832 – 837, 1956.
- [22] Surojit Saha, Sarang C. Joshi, and Ross T. Whitaker. Matching aggregate posteriors in the variational autoencoder. In *ICPR (6)*, pages 428–444, 2024.
- [23] Christian Szegedy, Vincent Vanhoucke, Sergey Ioffe, Jon Shlens, and Zbigniew Wojna. Rethinking the inception architecture for computer vision. In *2016 IEEE Conference on Computer Vision and Pattern Recognition (CVPR)*, pages 2818–2826, 2016.
- [24] Ilya Tolstikhin, Olivier Bousquet, Sylvain Gelly, and Bernhard Schoelkopf. Wasserstein auto-encoders. In *International Conference on Learning Representations*, 2018.
- [25] Jakub Tomczak and Max Welling. Vae with a vampprior. In Amos Storkey and Fernando Perez-Cruz, editors, *Proceedings of the Twenty-First International Conference on Artificial Intelligence and Statistics*, volume 84 of *Proceedings of Machine Learning Research*, pages 1214–1223. PMLR, 09–11 Apr 2018.
- [26] Han Xiao, Kashif Rasul, and Roland Vollgraf. Fashion-mnist: a novel image dataset for benchmarking machine learning algorithms. *CoRR*, abs/1708.07747, 2017.

Appendix

A Assumptions for Theorem 3.1

We mainly borrow the terminologies and assumptions in [21] which is the pioneering work in measuring deviations of density function estimates. Note that [21] studied the asymptotic distribution of the quadratic functional $\int [f_n(t) - f(t)]^2 a(t) dt$ under appropriate weight function a and conditions as sampling size n approaches to infinity. In inequality (5), we just saw that the weight function is the reciprocal of prior density in our case. Assumptions **A1** – **A4** are listed as follows:

(A1): The kernel function K is bounded, integrable, symmetric (about 0) and $\int K(t) dt = 1$, $\int t^2 K(t) dt < \infty$, $\int K^2(t) dt < \infty$. Also, K either (a) is supported on an closed and bounded interval $[-B, B]$ and is absolutely continuous on $[-B, B]$ with derivative K' or (b) is absolutely continuous on the whole real line with derivative K' satisfying $\int |K'(t)|^k dt < \infty$, $k = 1, 2$. Moreover,

$$\int_{t \geq 3} |t|^{\frac{3}{2}} [\log(\log|t|)]^{\frac{1}{2}} [|K'(t)| + |K(t)|] dt < \infty$$

(A2): The underlying density f is continuous, positive and bounded.

(A3): Squared density $f^{1/2}$ is absolutely continuous and its derivative is bounded in absolute value.

(A4): The second derivative f'' exists and is bounded.

We can see that the Gaussian kernel satisfies those assumptions, indicating that the kernel density estimation theory also works for Gaussian VAE. Similarly, most priors and posteriors we listed in section 1 lie in conditions **A1** – **A4**, demonstrating the promising applications of kernel estimate theory in variants of VAE.

B Proofs

B.1 Proof of Lemma 3.2

For simplicity, we first consider the following constraints

$$K \geq 0, \quad \int K(t) dt = 1, \quad \int t K(t) dt = 0, \quad \int t^2 K(t) dt = \frac{1}{5}.$$

By the method of undermined multipliers, it's equivalent to minimize the following target functional without constraints:

$$\int K^2(t) + aK(t) + ct^2 K(t) dt,$$

with simplified constraints above and a, c are undermined real coefficients. We ignore the term $tK(t)$ as it does not contribute to the unconstrained target function now.

For fixed t , denote $y(K) = K^2 + aK + ct^2 K$, $(K \geq 0)$. Note that the quadratic function $y(K)$ achieves minimum when $K = -\frac{c}{2}t^2 - \frac{a}{2}$.

It follows that $y(K)$ is minimized subject to $K \geq 0$ by

$$K(t) = \begin{cases} -\frac{c}{2}t^2 - \frac{a}{2} & -\frac{c}{2}t^2 - \frac{a}{2} \geq 0 \\ 0 & -\frac{c}{2}t^2 - \frac{a}{2} < 0. \end{cases}$$

We can rewrite it as

$$K(t) = \begin{cases} A(B^2 - t^2) & |t| \leq B \\ 0 & \text{otherwise.} \end{cases}$$

for some number A, B . By simplified assumptions $\int tK(t)dt = 0, \int t^2K(t)dt = \frac{1}{5}$, we can find that $A = \frac{3}{4}, B = 1$.

Under general moment conditions in Lemma 3.2, optimal K^* can be written as

$$K^*(t) = \begin{cases} \frac{3}{4r} \left(1 - \left(\frac{t-\mu}{r}\right)^2\right) & |t - \mu| \leq r \\ 0 & \text{otherwise.} \end{cases}$$

by location-scale formula. In literature [7], this kernel is called Epanechnikov kernel. We put $1/5$ in front of the constraint of second moment in order to make the resulting support interval cleaner, which won't change the optimal kernel. The corresponding optimal value of $I(K)$ is $I(K^*) = \frac{3}{5r}$.

Plots of Standard Epanechnikov kernel and Guassian kernel

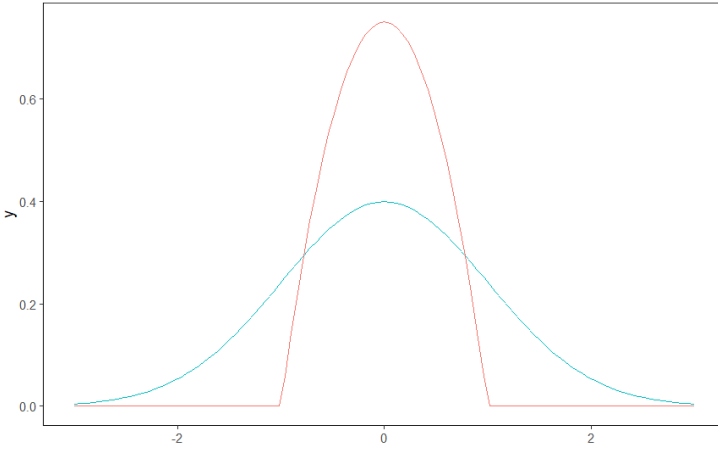


Figure S3: Red curve: Standard Epanechnikov kernel. Green curve: Standard Gaussian kernel.

B.2 Theoretical support for Algorithm 2

Given $U_1, U_2, U_3 \stackrel{i.i.d.}{\sim} \text{Unif}[-1, 1]$, we only need to show the density of $\text{median}(U_1, U_2, U_3)$ is standard Epanechnikov kernel.

Denote $Y = \text{Median}(U_1, U_2, U_3)$, we have

$$\begin{aligned} P(Y \leq t) &= P(\text{Median}(U_1, U_2, U_3) \leq t) \\ &= P(\text{Exactly two of } U_1, U_2, U_3 \text{ are less than } t) + P(\text{All of } U_1, U_2, U_3 \text{ are less than } t) \\ &= \binom{3}{2} \left(\frac{1+t}{2}\right)^2 \left(\frac{1-t}{2}\right) + \binom{3}{3} \left(\frac{1+t}{2}\right)^3 \\ &= \frac{1}{2} + \frac{3}{4}t - \frac{t^3}{4}. \end{aligned}$$

Then the density $f_Y(t)$ of Y is

$$f_Y(t) = \frac{3}{4} - \frac{3}{4}t^2 = \frac{3}{4}(1 - t^2),$$

which is essentially the standard Epanechnikov kernel.

C Model architecture

C.1 MNIST and Fashion-MNIST

We used fully convolutional architectures with 4×4 convolutional filters for both encoder and decoder in EVAE and VAE, as described following. All convolutions in the encoder and decoder employed SAME padding.

We resized images in MNIST and Fashion-MNIST from 28×28 to 32×32 at beginning. In the last conv layer, the sigmoid activation function was used to restrict the range of output as we assumed Bernoulli type model of $p_\theta(\mathbf{x}|\mathbf{z})$ and the binary cross entropy loss employed used (reduction to sum). Dimensions d_z for latent space : $\{8, 16, 32, 64\}$

Encoder q_ϕ :

$$\begin{aligned} x \in \mathbb{R}^{32 \times 32} &\rightarrow 32 \text{ Conv, Stride 2} \rightarrow \text{BatchNorm} \rightarrow \text{ReLU} \\ &\rightarrow 64 \text{ Conv, Stride 2} \rightarrow \text{BatchNorm} \rightarrow \text{ReLU} \\ &\rightarrow 128 \text{ Conv, Stride 2} \rightarrow \text{BatchNorm} \rightarrow \text{ReLU} \\ &\rightarrow 256 \text{ Conv, Stride 2} \rightarrow \text{BatchNorm} \rightarrow \text{ReLU} \\ &\rightarrow \text{Fully connected } (1 * 1 * 256 \times d_z) \text{ for each parameters} \end{aligned}$$

Decoder p_θ :

$$\begin{aligned} z \in \mathbb{R}^{d_z \times d_z} &\rightarrow \text{Fully connected } (d_z \times 1 * 1 * 256) \\ &\rightarrow 128 \text{ ConvTran, Stride 1} \rightarrow \text{BatchNorm} \rightarrow \text{ReLU} \\ &\rightarrow 64 \text{ ConvTran, Stride 2} \rightarrow \text{BatchNorm} \rightarrow \text{ReLU} \\ &\rightarrow 32 \text{ ConvTran, Stride 2} \rightarrow \text{BatchNorm} \rightarrow \text{ReLU} \\ &\rightarrow 1 \text{ ConvTran, Stride 2} \rightarrow \text{Sigmoid} \end{aligned}$$

C.2 CIFAR-10

Again, we used fully convolutional architectures with 4×4 convolutional filters for both encoder and decoder in EVAE and VAE for CIFAR-10 model. In encoder, we employed a layer of Adaptive Average pool filter. Other settings are the same with MNIST and Fashion-MNIST.

Encoder q_ϕ :

$$\begin{aligned} x \in \mathbb{R}^{32 \times 32} &\rightarrow 32 \text{ Conv, Stride 2} \rightarrow \text{BatchNorm} \rightarrow \text{ReLU} \\ &\rightarrow 64 \text{ Conv, Stride 2} \rightarrow \text{BatchNorm} \rightarrow \text{ReLU} \\ &\rightarrow 128 \text{ Conv, Stride 2} \rightarrow \text{BatchNorm} \rightarrow \text{ReLU} \\ &\rightarrow 256 \text{ Conv, Stride 2} \rightarrow \text{BatchNorm} \rightarrow \text{ReLU} \\ &\rightarrow \text{AdaptiveAvgPool2d} \\ &\rightarrow \text{Fully connected } (1 * 1 * 256 \times d_z) \text{ for each parameters} \end{aligned}$$

Decoder p_θ :

$$\begin{aligned} z \in \mathbb{R}^{d_z \times d_z} &\rightarrow \text{Fully connected } (d_z \times 1 * 1 * 256) \\ &\rightarrow 128 \text{ ConvTran, Stride 1} \rightarrow \text{BatchNorm} \rightarrow \text{ReLU} \\ &\rightarrow 64 \text{ ConvTran, Stride 2} \rightarrow \text{BatchNorm} \rightarrow \text{ReLU} \\ &\rightarrow 32 \text{ ConvTran, Stride 2} \rightarrow \text{BatchNorm} \rightarrow \text{ReLU} \\ &\rightarrow 3 \text{ ConvTran, Stride 2} \rightarrow \text{Sigmoid} \end{aligned}$$

C.3 CelebA

For CelebA dataset, we used 5×5 convolutional filters for both encoder and decoder in EVAE and VAE. Similar to CIFAR-10, we employed a layer of Adaptive Average pool filter before the fully connected layer in encoder. We first scaled images with Center Crop to 140×140 and resized them to 64×64 .

Encoder q_ϕ :

$$\begin{aligned}
 x \in \mathbb{R}^{64 \times 64} &\rightarrow 64 \text{ Conv, Stride 2} \rightarrow \text{BatchNorm} \rightarrow \text{ReLU} \\
 &\rightarrow 128 \text{ Conv, Stride 2} \rightarrow \text{BatchNorm} \rightarrow \text{ReLU} \\
 &\rightarrow 256 \text{ Conv, Stride 2} \rightarrow \text{BatchNorm} \rightarrow \text{ReLU} \\
 &\rightarrow 512 \text{ Conv, Stride 2} \rightarrow \text{BatchNorm} \rightarrow \text{ReLU} \\
 &\rightarrow \text{AdaptiveAvgPool2d} \\
 &\rightarrow \text{Fully connected } (1 * 1 * 512 \times d_z) \text{ for each parameters}
 \end{aligned}$$

Decoder p_θ :

$$\begin{aligned}
 z \in \mathbb{R}^{d_z \times d_z} &\rightarrow \text{Fully connected } (d_z \times 8 * 8 * 512) \\
 &\rightarrow 256 \text{ ConvTran, Stride 1} \rightarrow \text{BatchNorm} \rightarrow \text{ReLU} \\
 &\rightarrow 128 \text{ ConvTran, Stride 2} \rightarrow \text{BatchNorm} \rightarrow \text{ReLU} \\
 &\rightarrow 64 \text{ ConvTran, Stride 2} \rightarrow \text{BatchNorm} \rightarrow \text{ReLU} \\
 &\rightarrow 3 \text{ ConvTran, Stride 2} \rightarrow \text{Sigmoid}
 \end{aligned}$$

D Datasets and Training details

We list details for each benchmark dataset in following table

| Datasets | # Training samples | # Hold-out samples | Original image size |
|---------------|--------------------|--------------------|---------------------|
| MNIST | 60000 | 10000 | 28*28 |
| Fashion-MNIST | 60000 | 10000 | 28*28 |
| CIFAR-10 | 50000 | 10000 | 32*32 |
| CelebA | 162770 | 19867 | 178*218 |

Note that for MNIST, Fashion-MNIST and CIFAR-10, we used default splittings of training sets and testing sets provided in Pytorch (torchvision.datasets). For CelebA, we used default validation set as hold-out samples.

As to the training details, we used same training parameters for all algorithms and datasets, as described in following table

| | |
|-------------------------------|------------------------------|
| Latent space dimensions d_z | 8,16,32,64 |
| Optimizer | Adam with learning rate 3e-4 |
| Batch size | 100 |
| Epochs | 50 |

Calculation of Sharpness

We follow the way in [24] in calculating the sharpness of an image. For each generated image, we first transformed it into grayscale and convolved it with the Laplace filter $\begin{pmatrix} 0 & 1 & 0 \\ 1 & -4 & 1 \\ 0 & 1 & 0 \end{pmatrix}$, computed

the variance of the resulting activations and took the average of all variances. The resulting number is denoted as sharpness (larger is better). The blurrier image will have less edges. As a result, the variance of activations will be small as most activations will be close to zero. Note that we averaged the sharpness of all reconstructed images from hold-out samples for each dataset.

Binomial test for two models

If EVAE and VAE have similar performance in FID score, the probability that EVAE has lower FID score should be 0.5 in each independent experiment. (Same hypothesis for sharpness). However, according to Table 3 and 1, EVAE wins 15 experiments for FID score among all datasets. The p-value of winning 15 experiments under null hypothesis is

$$P(X \geq 15) = \binom{16}{16} (0.5)^{16} + \binom{16}{15} (0.5)^{16} \approx 2.6 \times 10^{-4} < 0.05.$$

P-value is smaller than 0.05 significance level thus EVAE significantly outperforms VAE in FID. Similar calculation can be applied to sharpness, whose p-value of winning 12 experiments is $P(X \geq 15) = \sum_{i=15}^{16} \binom{16}{i} 0.5^{16} \approx 2.6 \times 10^{-4} < 0.05$ and we achieved the same conclusion for the significance of EVAE's superiority in sharpness.

E Sampled reconstructed images

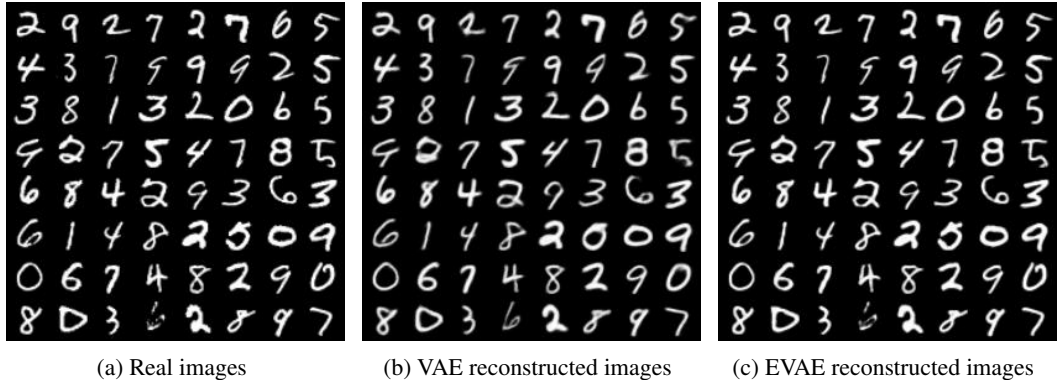


Figure S4: (a) Sampled real images from hold-out samples in MNIST (b) Reconstructed images by VAE. (c) Reconstructed images by EVAE. Dimension $d_z = 64$ for both models. See section C for Model architectures.

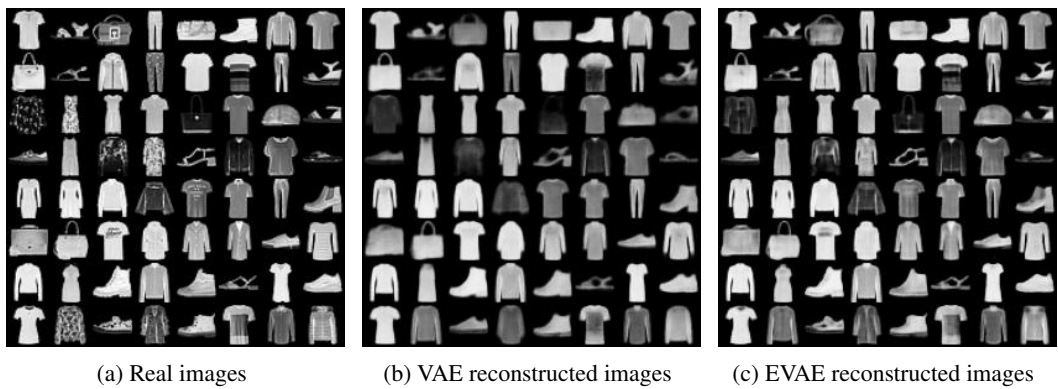


Figure S5: (a) Sampled real images from hold-out samples in Fashion-MNIST (b) Reconstructed images by VAE. (c) Reconstructed images by EVAE. Dimension $d_z = 64$ for both models.



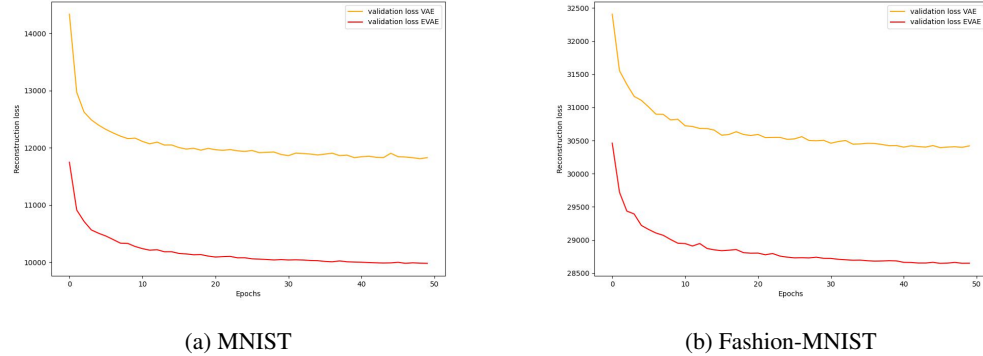
(a) Real images

(b) VAE reconstructed images

(c) EVAE reconstructed images

Figure S6: (a) Sampled real images from hold-out samples in CelebA (b) Reconstructed images by VAE. (c) Reconstructed images by EVAE. Dimension $d_z = 64$ for both models.

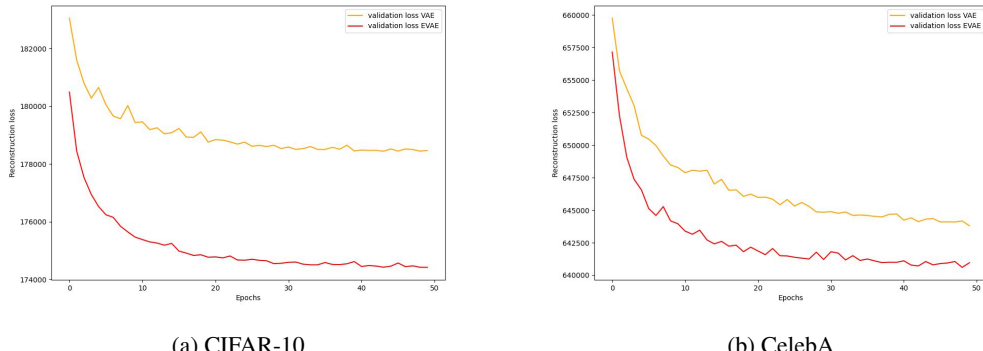
F Validation curves



(a) MNIST

(b) Fashion-MNIST

Figure S7: Reconstruction validation loss curves as function of Epochs. ($d_z = 64$). Red curve is for EVAE and yellow one represents VAE. Binary cross entropy loss is reduced to sum for each batch (a) MNIST (b) Fashion-MNIST.



(a) CIFAR-10

(b) CelebA

Figure S8: Reconstruction validation loss curves as function of Epochs. ($d_z = 64$). Red curve is for EVAE and yellow one represents VAE. Binary cross entropy loss is reduced to sum for each batch (a) CIFAR-10 (b) CelebA.

G More experiment details on EVAE

G.1 Benchmark datasets

For comparison, we applied a classical CNN architecture (Appendix C) in encoding and decoding part for all datasets. Consequently, the main differences between EVAE and VAE in implementation stem from the resampling step and target function in training procedure. All FID scores and sharpness are based on hold-out samples. We also evaluated VAE and EVAE with different dimensions d_z of latent spaces. Table 1 summarize the results on CIFAR10 and CelebA datasets with uniform prior support parameter $B=0.1$ in EVAE. More results for MNIST and Fashion-MNIST can be found in Table 3

Table 3: VAE and EVAE results on MNIST and Fashion-MNIST datasets

| Datasets | MNIST | | | | Fashion-MNIST | | | |
|----------|-------|--------|-----------|--------|---------------|--------|-----------|--------|
| | d_z | VAE | | EVAE | | VAE | | EVAE |
| | | FID | Sharpness | FID | Sharpness | FID | Sharpness | FID |
| 8 | 15.70 | 0.0211 | 14.74 | 0.0243 | 41.47 | 0.0157 | 36.18 | 0.0176 |
| 16 | 11.93 | 0.0252 | 10.49 | 0.0305 | 38.85 | 0.0159 | 26.71 | 0.0216 |
| 32 | 11.97 | 0.0249 | 7.92 | 0.0338 | 38.74 | 0.0163 | 18.47 | 0.0251 |
| 64 | 11.97 | 0.0246 | 5.13 | 0.0360 | 39.31 | 0.0161 | 12.02 | 0.0267 |

G.2 EVAE with Gaussian prior

To check whether the superior performance of EVAE over Gaussian VAE comes from the new prior (uniform) or new posterior (convolution between prior and KDE), we performed extra experiments for EVAE with Gaussian prior. Table 4 and Table 5 in Appendix G.2 compare the FID score and sharpness of EVAE (with Gaussian prior and $B=0.1$) with VAE and results show that EVAE still outperforms VAE. To this point, we can say the superior performance of EVAE mainly comes from the introduction of KDE based posterior.

The experiment details are the same with Appendix C. The only difference is we replaced uniform prior with Gaussian prior and we still kept the support parameter $B(=0.1)$ in front of Gaussian prior.

Table 4: VAE and EVAE results on MNIST and Fashion-MNIST datasets

| Datasets | MNIST | | | | Fashion-MNIST | | | |
|----------|-------|--------|-----------|--------|---------------|--------|-----------|--------|
| | d_z | VAE | | EVAE | | VAE | | EVAE |
| | | FID | Sharpness | FID | Sharpness | FID | Sharpness | FID |
| 8 | 16.14 | 0.0217 | 15.22 | 0.0246 | 42.22 | 0.0157 | 35.89 | 0.0181 |
| 16 | 12.11 | 0.0248 | 10.25 | 0.0308 | 38.88 | 0.0167 | 26.65 | 0.0218 |
| 32 | 12.43 | 0.0247 | 8.22 | 0.0335 | 39.14 | 0.0157 | 18.52 | 0.0246 |
| 64 | 11.73 | 0.0248 | 5.74 | 0.0364 | 38.96 | 0.0159 | 12.18 | 0.0271 |

Table 5: VAE and EVAE results on CIFAR10 and CelebA datasets

| Datasets | CIFAR-10 | | | | CelebA | | | |
|----------|----------|--------|-----------|--------|-----------|--------|-----------|--------|
| | d_z | VAE | | EVAE | | VAE | | EVAE |
| | | FID | Sharpness | FID | Sharpness | FID | Sharpness | FID |
| 8 | 228.92 | 0.0353 | 218.84 | 0.0355 | 194.36 | 0.0149 | 194.62 | 0.0145 |
| 16 | 183.03 | 0.0360 | 163.84 | 0.0355 | 144.88 | 0.0155 | 147.78 | 0.0157 |
| 32 | 146.80 | 0.0359 | 122.17 | 0.0364 | 106.02 | 0.0160 | 102.73 | 0.0163 |
| 64 | 141.22 | 0.0353 | 79.06 | 0.0356 | 80.60 | 0.0161 | 65.79 | 0.0164 |

G.3 Effect of uniform prior support parameter B

Table 6 summarizes the performance of EVAE with uniform prior under different values of B in different datasets. ($d = 64$ and other settings are the same with original experiments). We can see EVAE becomes worse when B is relatively large. One reason maybe that prior distribution with larger support is likely to generate outlier samples and lower down the quality of reconstructed sample. Additionally, the large value of B will add more weight on the regularization term of the new target function (10) of EVAE, which trades off the reconstruction performance of EVAE.

Table 6: The **FID** score of EVAE with different constant value of B in MNIST, Fashion-MNIST and CIFAR-10 datasets. ($d_z = 64$ in all cases)

| Support parameter B | MINST | Fashion-MNIST | CIFAR-10 |
|---------------------|-------|---------------|----------|
| B = 0.01 | 4.96 | 12.2 | 81.1 |
| B = 0.1 | 5.14 | 12.4 | 79.4 |
| B = 1 | 7.13 | 16.9 | 93.9 |
| B = 10 | 11.29 | 33.7 | 153.3 |
| B = 20 | 12.93 | 43.1 | 168.7 |

G.4 Time efficiency of EVAE

One advantage of kernel posterior proposed in equation (11) is that the quadratic functional $I(K)$ has a closed form for many distributions, while the closed form of KL divergence in standard ELBO can be hard to derive when we want to use complicated posterior and prior. For example, the KL divergence becomes piecewise for the uniform prior and posterior. In those cases, time-consuming Monte Carlo simulations might be needed.

To explore the time efficiency of EVAE, we performed additional experiments in Table G.4 to compare the average and standard error of the training time (in seconds) per epoch (10 epochs total for each experiment) for VAE and EVAE in CIFAR10 and CelebA-64.

Table 7: Training time of EVAE and VAE per epoch in seconds

| Latent space dimension d_z | CIFAR10 | | CelebA-64 | |
|------------------------------|------------|------------|--------------|--------------|
| | VAE(std) | EVAE(std) | VAE(std) | EVAE(std) |
| $d_z = 8$ | 7.21(0.28) | 7.9(0.19) | 208.94(5.95) | 208.42(4.33) |
| $d_z = 16$ | 7.22(0.43) | 7.99(0.19) | 209.10(5.94) | 210.88(5.35) |
| $d_z = 32$ | 7.9(0.6) | 8.87(0.31) | 208.02(3.22) | 210.23(2.81) |
| $d_z = 64$ | 7.56(0.4) | 8.56(0.63) | 206.85(5.24) | 207.72(5.66) |

In general, we found that EVAE has the comparable time efficiency to VAE. The slight increase in training time for EVAE results from the sampling process of the Epanechnikov kernel, which requires a few more samples to achieve the Epanechnikov density, as described in Algorithm 2. The difference in training time is negligible when the latent space dimension is large, which facilitates the application of EVAE in high-resolution datasets.

H Broader Impact Statement

This paper aims to propose a new perspective in modeling the posterior in generative models by kernel density estimations. The theoretical results should not have negative societal impacts. One possible negative impact resulting from EVAE might be the misuse of generative models in producing fake images which may lead to security issues in some face recognition based systems. Few mitigation strategies: (1) gate the release of models for commercial use; (2) add a mechanism for monitoring fake images generated by models such as the discriminator in GAN models. We can also restrict the private datasets used in training the generative model. All benchmark datasets used in this paper are public and well known to the machine learning community.